Available online at www.sciencedirect.com
ScienceDirect
Nuclear Instruments and Methods in Physics Research A 580 (2007) 938–943
NUCLEAR INSTRUMENTS & METHODS IN PHYSICS RESEARCH Section A
www.elsevier.com/locate/nima

ISPMER: Integrated system for combined PET, MRI, and electrophysiological recording in somatosensory studies in rats

Yen-Yu Shih[a], You-Yin Chen[b], Jyh-Cheng Chen[c,e], Chen Chang[d], Fu-Shan Jaw[a,*]

[a]*Institute of Biomedical Engineering, National Taiwan University, No. 1, Section 4, Roosevelt Road, Taipei, Taiwan*
[b]*Department of Electrical and Control Engineering, National Chiao-Tung University, Hsinchu, Taiwan*
[c]*Faculty of Biomedical Imaging and Radiological Sciences, National Yang-Ming University, Taipei, Taiwan*
[d]*Institute of Biomedical Sciences, Academia Sinica, Taipei, Taiwan*
[e]*Department of Education and Research, Taipei City Hospital, Taipei, Taiwan*

Available online 30 June 2007

Abstract

The present study developed an integrated system for use in combined PET, MRI, and electrophysiological recording in somatosensory studies in rats, called ISPMER. A stereotaxic frame was designed for animal positioning that could be used in all three measurement modalities, and its dimensions complied with the gold standard of the Paxinos and Watson rat brain atlas. A graphical user interface was developed for analyzing the data using several signal processing algorithms. This integrated system provides a novel interface for the recording and processing of three-dimensional neuronal signals in three modalities.

PACS: 87.57.−s

Keywords: PET; MRI; Electrophysiology; Stereotaxic frame; Rat

1. Introduction

Somatosensory studies in rats provide important information about neuronal signal processing in the central nervous system [1,2]. Electrophysiological techniques are commonly used to record neuronal activities in neuroscience research. Methods such as single-unit recording and field potential (FP) recording exhibit an outstanding temporal resolution, of the order of milliseconds [3,4], but they do not have the capability to record over a wide region within a short time frame. However, such spatial recording can be achieved using functional imaging techniques, such as positron-emission tomography (PET) and functional magnetic resonance imaging (fMRI).

PET is a non-invasive imaging method that provides functional information by detecting the distribution of a positron emitter throughout an region of interest (ROI). The first tomographic measurement using ^{18}F-fluorodeoxyglucose (^{18}F-FDG) was made by Phelps et al. in 1979, who reported its use in mapping the cerebral metabolic rate of glucose [5].

In 1990, Ogawa et al. [6,7] proposed the blood-oxygenation-level-dependent (BOLD) fMRI method based on hemodynamic responses. BOLD fMRI is based on the presence of a paramagnetic substance, such as deoxyhemoglobin (Hb), that can interfere with the magnetic field so as to reduce the intensity of signals. Activation of neurons can stimulate vasodilatation indirectly and overcompensate the regional cerebral blood flow so as to introduce more oxygen and glucose. This causes the ratio of paramagnetic deoxy-Hb in blood to be reduced when the neural activity increases, resulting in more intense signals in activated brain areas [8–10].

Unlike single-unit recording, FP recording can provide macrocosmic information about neurons. The integrated electrical signals reflect volume conduction of multiple neuronal activities, and hence FPs can be used to observe the activities of groups of neurons. This technique also provides relative information anatomically, that is, the

*Corresponding author. Tel.: +886 2 33665266.
E-mail address: jaw@ha.mc.ntu.edu.tw (F.-S. Jaw).

0168-9002/$ - see front matter © 2007 Elsevier B.V. All rights reserved.
doi:10.1016/j.nima.2007.06.062

source of each signal that generates FPs. Thus, the present study applied the above technique to demonstrate the distributions and functions of areas excited by specific stimuli.

The different types of data described above are difficult to correlate with each other due to localization errors and incompatibility of the different data analysis software used for each. This prompted us to develop an integrated system for PET, MRI, and electrophysiological recording (ISPMER) consisting of a stereotaxic frame and a data analysis interface in order to combine the advantages of these three modalities and provide an interface that integrates the various functional responses. In the present study, the ^{18}F-FDG-microPET, BOLD microMRI, and electrophysiological recording techniques were used to elucidate evoked responses in the rat brain.

2. Experiments

2.1. Stereotaxic frame for measurements of the rat brain

The body of stereotaxic frame of the ISPMER system is constructed from acrylic, the screw is made of Nylon 66, and the incisor fixer is made of polypropylene so as to reduce attenuation and scattering of γ-ray photons during PET scans, and to avoid magnetic interference during MRI scans (Fig. 1). The bottom of the frame is flat to facilitate electrophysiological experiments. Two ear bars with a tip of 16° and an incisor fixer are used to position the rat head, with tapes used to restrain the body. The rat head can be fixed firmly to the stereotaxic frame with two ear bars in an identified interaural line through the external auditory meatus. The incisors are fixed at 3.3 mm below the horizontal interaural line. Gas anesthesia can be administered through the incisor fixer, with an oral–nasal airbag mask used to keep the gas around the head. The bregma is taken as a landmark in the rat brain, which is 9 mm anterior to the midpoint of the two ear bars. The spatial design of the stereotaxic frame is compatible with a small-animal stereotaxic frame from David Kopf Instruments that is commonly used in electrophysiological recordings, and the slice orientations of the PET and MRI images are identical to those in the Paxinos and Watson rat brain atlas [11].

2.2. microPET

For microPET (R4, Concorde Microsystems, Knoxville, TN, USA) imaging, rats were lightly restrained, and an electrical stimulus (1 Hz, 5–10 V pulses of 100 μs duration) was applied to the left hind paw during the 45 min uptake period after injecting 3–3.5 mCi of ^{18}F-FDG. Quantitative dynamic scanning was performed on each rat for 30 min. Three-dimensional (3D) volumetric images were acquired in 1 min frames using standard 3D filtered back-projection reconstruction.

2.3. MRI

Magnetic resonance (MR) images were obtained using a 4.7-T system (Biospec BMT 47/40, Bruker). Forty–four slice gradient echo images (TR = 215 ms, TE = 20 ms, flip angle = 22.5°, FOV = 4 cm, SLTH = 2 mm, NEX = 2, and acquisition matrix = 256 × 64 pixels [256 × 256 pixels after zero-padding]) were acquired at the same position, with each frame taking 27 s. The first 20 consecutive frames were collected as a baseline, and the second 20 were collected during the stimulation.

2.4. Electrophysiological experiments

After acquiring functional images using microPET and MRI, evoked potentials in response to stimulation of the left hind paw were recorded using FP recording. The rats were anesthetized by continuous delivery of low-dosage ketamine using an infusion pump (15 mg/ml, 1 ml/h, i.v.). The detected evoked FPs were amplified 2500 times, filtered from 0.01 to 300 Hz, and digitized at 3000 Hz by an A-to-D converter card (PCI-MIO-16E-4, National Instruments, TX, USA).

2.5. Current-source-density (CSD) analysis

CSD analysis identifies the sites of current flow in neuronal tissues [12], and has been used to reveal physiological and anatomical aspects of neuronal circuits [13–15] based on the spatiotemporal distribution of activated sinks (inward membrane currents in the extracellular space) and sources (outward membrane currents). In the present study, the two-dimensional (2D) CSD analysis assumed that dipole-producing currents flow in the coronary section (mainly along the stereotaxic x and z coordinates), which were calculated according to

$$-I_m = \sigma_x \frac{\partial^2}{\partial x^2}\phi + \sigma_z \frac{\partial^2}{\partial z^2}\phi \tag{1}$$

where I_m is the net current; σ_x and σ_z are the tissue conductivities along the x (mediolateral) and z (dorsoventral) axes, respectively; and ϕ is the FP.

Five-point smoothing was applied to the second spatial derivative of the FP due to spatial sampling variability:

$$-I_m \approx \frac{1}{4\Delta d^2}\left(\sigma_x \sum_{m=-2}^{m=2} a_m \phi(x + m\Delta d) + \sigma_z \sum_{m=-2}^{m=2} a_m \phi(z + m\Delta d)\right), \tag{2}$$

where Δd is the sampling interval (50 μm), $a_0 = -2$, $a_{\pm 1} = 0$, and $a_{\pm 2} = 1$.

2.6. Image analysis

The image processing interface was constructed in MATLAB (version 7). Its functions include automatic

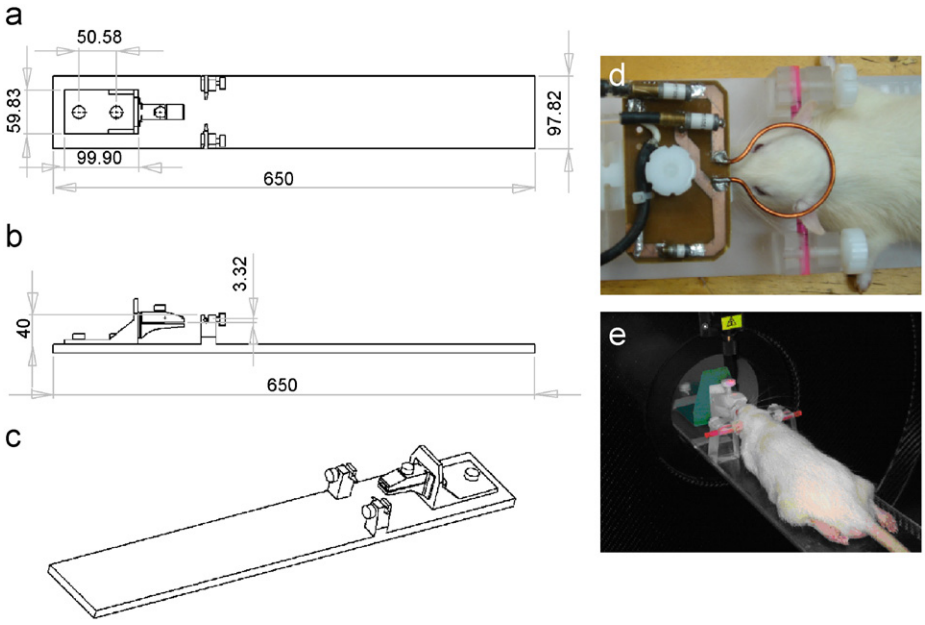

Fig. 1. (a)–(c) Schematics of the stereotaxic frame; (d) Rat positioned in the stereotaxic frame, to which the MRI coil is fixed; (e) Rat in the small-animal stereotaxic frame that is attached to the microPET bed.

atlas-based ROI and volume of interest calculations, time–activity curve (TAC) analysis, parametric image analysis, cross-correlation analysis, statistical image mapping, movie display, multiple-subjects image analysis, FP, CSD, 3D surface rendering, and manual image registration and fusion using scaling and shifting operations (Fig. 2).

For dynamic MR images, the TAC and the input stimulation paradigm were calculated using the correlation coefficient technique according to the following equation and Fig. 3:

$$C(x,y)=\frac{\sum_{t=1}^{N}[P(x,y,t)-\mu_{\mathrm{P}}(x,y)][R(t)-\mu_{\mathrm{R}}]}{\sqrt{\sum_{t=1}^{N}[P(x,y,t)-\mu_{\mathrm{P}}(x,y)]^2}\sqrt{\sum_{t=1}^{N}[R(t)-\mu_{\mathrm{R}}]^2}}, \tag{3}$$

where $R(t)$ is the function of the input paradigm, $P(x, y, t)$ is the TAC, $\mu_{\mathrm{P}}(x, y)$ is the mean of $P(x, y, t)$, and μ_{R} is the mean of $R(t)$.

After mapping the correlation coefficient onto high-resolution MR template images, the results were transformed from 3D dynamic data to 2D functional maps (Figs. 4a and b). For microPET images, the data were initially registered and fused with a high-resolution MRI template by normalizing the pixel size. The atlas and high-resolution PET/MRI images were then registered and fused using manual scaling and shifting operations based on the edges of the images (Fig. 4c). The shifting operation represents a translation of the matrix, with all the contents of the image moved by the same distance and the areas outside the original image filled with zeroes. This process does not change the values of the original pixels, only their positions in the image. For the scaling operation, each image was trimmed or enlarged and then resized using a bicubic transformation. Both methods were applied at the level of the pixel.

A novel automatic atlas-based ROI selection technique was implemented by precisely defining the coordinates of each brain area in the digital rat brain atlas. The relative coordinates of the brain area were simultaneously warped during the registration process, allowing a precise ROI to be selected automatically. This technique can be used to reveal the activated voxels in each brain area and generate the data in ROIs for further statistical analyses. Multiple-subject image analysis is an advanced digital atlas technique that was used to compare the data among animals, with the results combined into a single map called the incidence image (Fig. 4d). Registering each image to the atlas template eliminates spatial errors, and allows the average image of each normalized subject to be obtained. Furthermore, electrophysiological recording areas in the thalamus were mapped by referencing the rat atlas. The FP and CSD evoked by electrical stimulation of the rat hind paw are shown in Fig. 4e.

3. Discussions

The novel feature of the ISPMER is the integration of three measurement modalities: PET, MRI, and electrophysiological recording. The use of the same stereotaxic frame in all the three modalities facilitates constant positioning throughout a sequence of experiments, thus reducing localization errors. We used the Paxinos and Watson rat brain atlas as the gold standard for the central nervous system of rats. Many studies have used atlas-image registration techniques to define responsive areas [2,16]. However, most conventional stereotaxic frames neglect the spatial relationship between the interaural line and

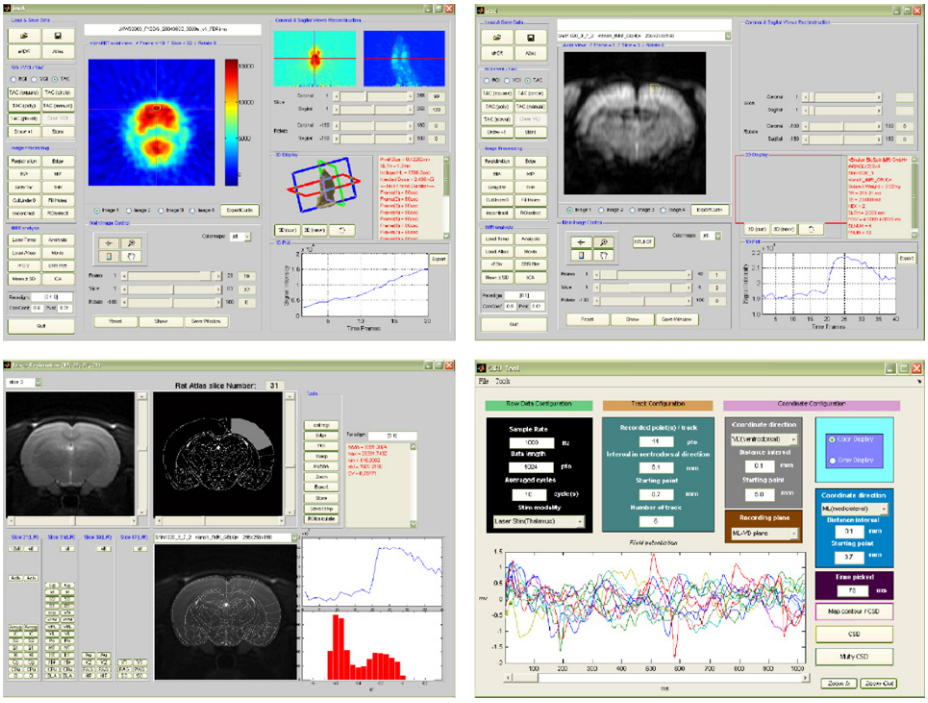

Fig. 2. Interface for analyzing PET, MRI, and electrophysiological recording data.

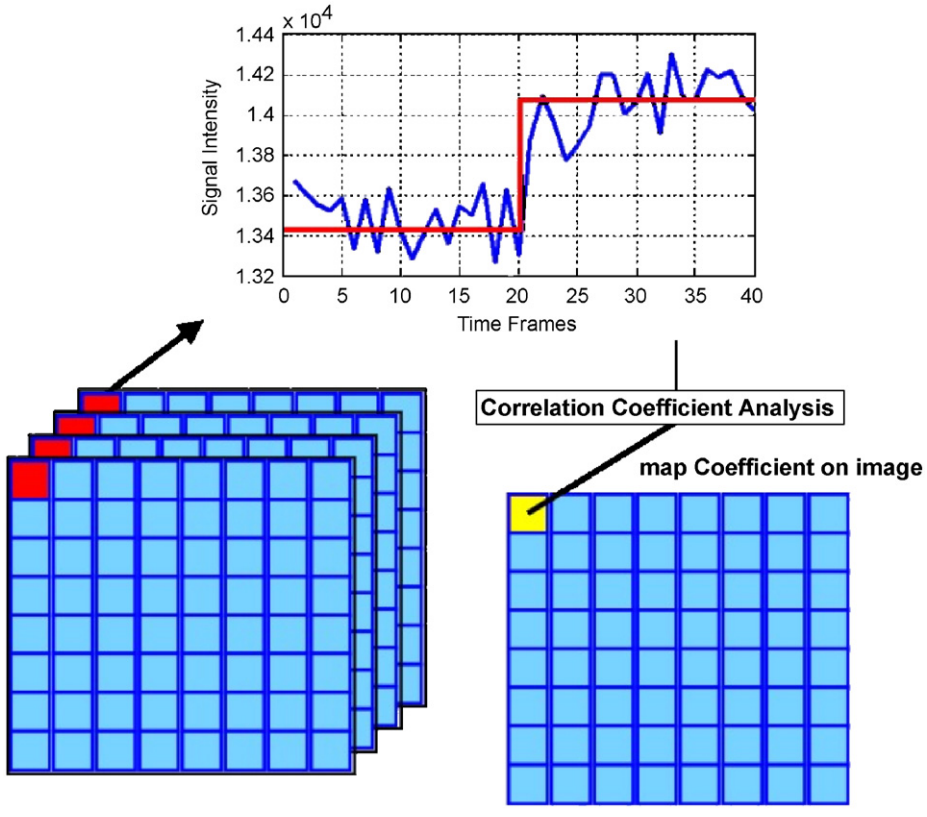

Fig. 3. For dynamic MRI images, the TAC and the input stimulation paradigm were calculated using the correlation coefficient technique on a pixel-by-pixel basis.

incisors. In adult rats, a flat-skull position can be achieved only when the incisor bar is lowered to 3.3 ± 0.4 mm in the horizontal direction. It is important to apply this calibration before imaging, since a non-flat image prevents precise definition of the local neuronal activation when referring to an atlas. Since the rat brain is small, a small

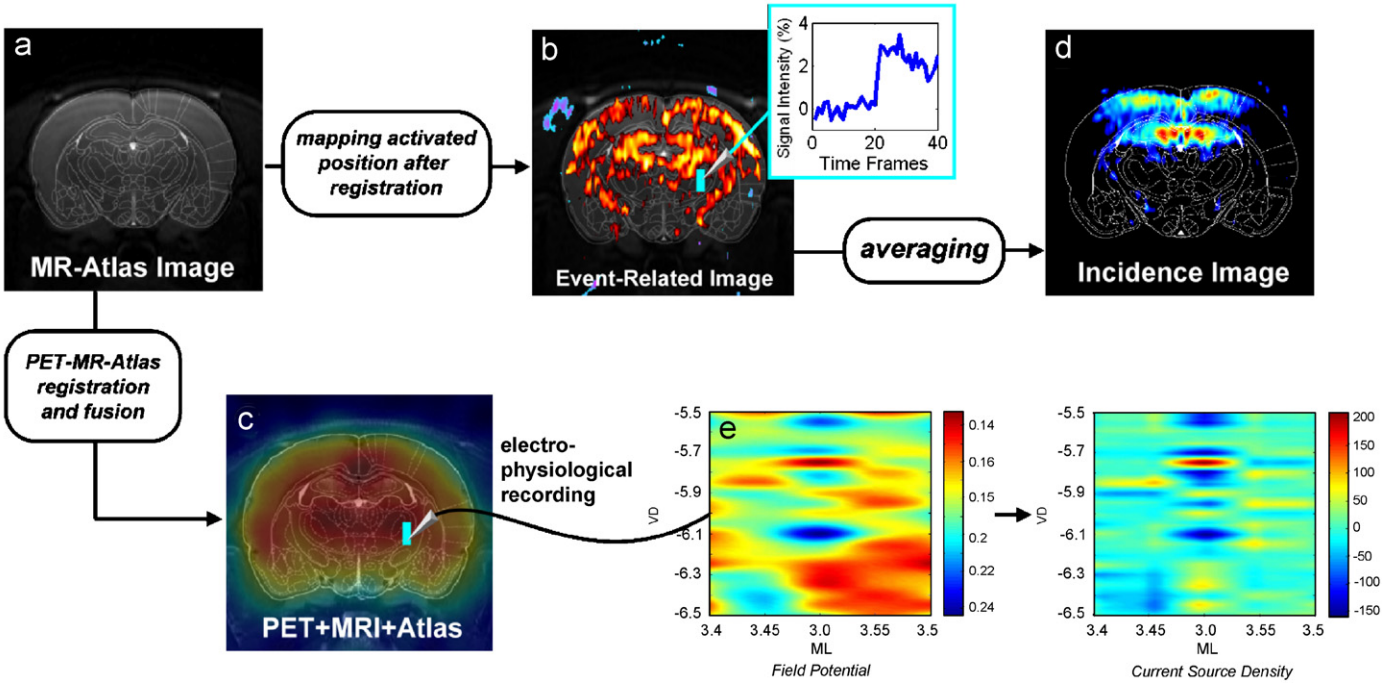

Fig. 4. (a) Images from MRI and the rat brain atlas were registered by scaling and shifting operations; (b) event-related signals superimposed on the image in (a) and the corresponding TAC; (c) microPET data co-registered with image in (a); (d) incidence images calculated by averaging the correlation coefficient maps of several subjects during simulation. Each correlation map was normalized to the domain of the rat brain atlas before averaging; (e) FP and CSD maps of the area in the ventral posterolateral thalamic nucleus that responded to stimulation of the left hindpaw.

error in elevation in the registration process can cause major discrepancies. Thus, precise positioning of rat head is crucial to obtaining consistent spatial alignment in different measurement modalities.

As mentioned above, the dimensions of the stereotaxic apparatus were designed to produce images identical to those in the Paxinos and Watson rat brain atlas. Since the spatial location of the head restrainer was identical to that in the stereotaxic frame from David Kopf Instruments, the accuracy was also the same. A similar study has used an identical spatial system with a pair of sharp or blunt ear bars to reposition animals in serial microPET imaging protocols [17]. Since high reproducibility was reported for that spatial system, we did not perform an accuracy test in the present study.

We used spatial shifting and bicubic interpolation as the scaling method to register data obtained from the three measurement modalities. Bicubic interpolation is one of the most widely used scaling techniques, and is commonly used to scale lesions in MR images [18]. In order to minimize interindividual bias, all registrations and analyses were performed by a single person in this study. Although manual registration is not an ideal method, Fig. 4a indicates that it is sufficiently accurate.

Unlike manual ROI techniques, our novel automatic atlas-based ROI selection accurately measures the regional radioactivity, and provides high-spatial-resolution MRI images and high-temporal-resolution FP signals. This resolves the disadvantage of each recording method by combining their results in a systematic manner. Each subject was precisely registered to the rat brain atlas, and our data demonstrated the efficacy of combining ISPMER with atlas-based normalization.

Acknowledgments

This work was supported by Grant no. NSC-94-2213-E-002-001 from the National Science Council, Taiwan, ROC. The authors acknowledge the technical support from the Functional and Micro-Magnetic Resonance Imaging Center and the Molecular-Genetic Imaging Core, which are supported by the National Research Program for Genomic Medicine of the National Science Council, Taiwan, ROC (Nos. NSC95-3112-B-001-009 and NSC95-3112-B-001-004).

References

[1] C. Spenger, A. Josephson, T. Klason, M. Hoehn, W. Schwindt, M. Ingvar, L. Olson, Exp. Neurol. 166 (2000) 246.
[2] S.D. Keilholz, A.C. Silva, M. Raman, H. Merkle, A.P. Koretsky, Magn. Reson. Med. 55 (2006) 316.
[3] D.H. Hubel, T.N. Wiesel, J. Physiol. 195 (1968) 215.
[4] G. Buzsáki, R.G. Bickford, L.J. Ryan, S. Young, O. Prohaska, R.J. Mandel, F.H. Gage, J. Neurosci. Methods 28 (1989) 209.
[5] M.E. Phelps, S.C. Huang, E.J. Hoffman, C. Selin, L. Sokoloff, D.E. Kuhl, Ann. Neurol. 6 (1979) 371.
[6] S. Ogawa, T.M. Lee, A.S. Nayak, P. Glynn, Magn. Reson. Med. 14 (1990) 68.
[7] S. Ogawa, T.M. Lee, A.R. Kay, D.W. Tank, Proc. Natl. Acad. Sci. USA 87 (1990) 9868.
[8] N.K. Logothetis, J. Pauls, M. Augath, T. Trinath, A. Oeltermann, Nature 412 (2001) 150.

[9] F. Hyder, I. Kida, K.L. Behar, R.P. Kennan, P.K. Maciejewski, D.L. Rothman, NMR Biomed. 14 (2001) 413.
[10] D.J. Heeger, D. Ress, Nat. Rev. Neurosci. 3 (2002) 142.
[11] G. Paxinos, C. Watson, The Rat Brain in Stereotaxic Coordinates, Academic Press, San Diego, CA, 1998.
[12] U. Mitzdorf, Physiol. Rev. 65 (1985) 37.
[13] V.A. Aroniadou, A. Keller, J. Neurophysiol. 70 (1993) 1553.
[14] N.A. Lambert, A.M. Borroni, L.M. Grover, T.J. Teyler, J. Neurophysiol. 66 (1991) 1538.
[15] U. Mitzdorf, W. Singer, Exp. Brain Res. 33 (1978) 371.
[16] Y.B. Shah, L. Haynes, M.J. Prior, C.A. Marsden, P.G. Morris, V. Chapman, Psychopharmacology 180 (2005) 761.
[17] D.J. Rubins, A.K. Meadors, S. Yee, W.P. Melega, S.R. Cherry, J. Neurosci. Methods 107 (2001) 63.
[18] E.R. Melhem, E.H. Herskovits, K. Karli-Oguz, X. Golay, D.A. Hammoud, B.J. Fortman, F.M. Munter, R. Itoh, AJR Am. J. Roentgenol. 180 (2003) 65.